Investigation of the Unsteady Flow in a Counter-Rotating Compressor Using the Nonlinear Harmonic Method

Wang Lei[*1] Liu Bo[2]
[*1]recoba201@g mail.com; [2]liubo704@nwpu.edu.cn;

***Abstract*-In the present paper, the Nonlinear Harmonic (NLH) method implemented in Fine/Turbo code has been evaluated for unsteady rotor-rotor interaction analysis. Strengths and weaknesses of the NLH method are highlighted through direct comparison with experimental data and time-domain unsteady simulation for the NWPU counter-rotating research compressor (CRRC) at the design and off-design conditions. The rotor-rotor interactions were studied in detail to advance the understanding of the flow physics involved. Based on the unsteady simulation, deterministic stresses were computed and compared to the NLH method to analyze distinct sources of unsteadiness and their effect on the time-averaged flow field. For the present case, the NLH method is about one order magnitude faster than the direct time-domain method.**

Keywords-Counter-rotating; Rotor-rotor Interaction; Harmonic; Deterministic Stress

I. INTRODUCTION

The current generation of high performance fans and compressors are being designed with the goal of maximizing blade loading and minimizing blade row spacing in order to increase performance and reduce compressor length and thus weight. Counter-rotation, as one of the promising technologies in lowering engine weight, has become more and more attractive for substantial improvement in aerodynamic performance. By counter rotation the pressure ratio can be increased substantially without needing high circumferential speed in the individual blade rows because the sum of the circumferential velocities of two adjacent blade rows is available for the work input. The stator could be cancelled from the compressor and the torque of the two shafts in a counter-rotating system is less than half of that in a single shaft system [1]. The result is a potential for higher pressure ratios with fewer blade rows, hence either shorter or lighter compressors. Applications for counter-rotating technology do have the potential to be an alternative propulsor for future very high bypass engines and in high-supersonic cruise aircraft [2-3].

II. NONLINEAR HARMONIC METHOD

The time-domain method to solve unsteady flow fields in multistage turbomachines can provide insights to help our understanding of complex unsteady flow phenomena. However, due to unequal blade counts in neighboring bladerows, an unsteady calculation has to be carried out in multiple passages/whole annulus owing to the required direct periodic condition. Moreover, it is recognized that the time-domain unsteady simulation is difficult to extract useful information and prohibitively expensive in computational time, which, in an engineering context, can constitute a major limitation. Therefore it is not feasible to be used in a routine design and explains why steady simulation is still widely used at industrial framework.

The development of efficient unsteady aerodynamic modeling methodologies has been an active research area. In order to overcome that problem, the sophisticated frequency domain approach has been extended into the multistage turbomachiny to predict blade row interactions. He[4] proposed a nonlinear harmonic (NLH) method that revealed superior to the time-domain unsteady simulation.

The main idea in NLH method is that an unsteady flow variable can be decomposed into a time-averaged part and a sum of periodic perturbations, which in turn can be decomposed into N harmonics.

$$U(\vec{r},t)=\bar{U}(\vec{r})+\sum U'(\vec{r},t) \qquad (1)$$

$$U'(\vec{r},t)=\sum_{k=1}^{N}\left(\tilde{U}_k(\vec{r})e^{I\omega_k t}+\tilde{U}_{-k}(\vec{r})e^{I\omega_{-k}t}\right) \qquad (2)$$

Where $\bar{U}(\vec{r})$ is the time-averaged part, $U'(\vec{r},t)$ is the unsteady part induced by the unsteady disturbance. The unsteady disturbances are caused by blade passing frequency of the adjacent rotating blade row. These periodically perturbations are transformed into the frequency domain by a Fourier transform, which represents the oscillating influence of the perturbations caused by the adjacent rows. The accuracy of the solution is determined by the number of harmonics and, especially for multi-stage environment, the number of perturbations or blade passing frequencies. It is highly desired that this algorithm solve for the periodic solution directly, avoiding the expensive transients typical of time-domain schemes and consume most of the CPU resources.

The so-called deterministic stress terms due to nonlinearity of the momentum and energy equations were solved simultaneously with the harmonic perturbation equations in a strongly coupled approach. These terms are similar to the Reynolds stress terms, which can account for the nonlinear effects of unsteadiness on the time-averaged flow, making this approach similar to the average-passage method of Adamczyk[5]. The important advantage of the method is that the extra deterministic stress is calculated directly from products of the real parts and imaginary parts of the complex amplitudes [6].

III. FOCUS OF RESEARCH EFFORT

The NLH method has been tested and validated against several turbomachinery cases, with the result that the time savings seemed to be significant over the time-domain unsteady method [6-7]. The first priority of present study is directed toward demonstrating those claims in a counter-rotating research compressor, as the NLH method is relatively new with limited validation. Apart from this, there are several issues of interest. First, the performance maps of NLH method results are verified by comparison with experimental data. Second, considering that the validation of a 3-D unsteady flow structure is much more difficult than its steady counterpart because of the extreme difficulty to obtain detailed unsteady data to provide quantitative measurement and visualization of flow structure in CRRC. Therefore, to demonstrate the accuracy and computational efficiency of the NLH method, it is also compared to a time-domain unsteady simulation to advance our present understanding of the complicated interactions between rotors, which is deemed to be a real challenge to the NLH method.

IV. EXPERIMENTAL FACILITY

The numerical test rig in this work is a counter-rotating research compressor (CRRC) at the NWPU National Defense Aerodynamics Laboratory of Airfoil and Cascade, which is shown in Fig. 1. Over the past three years we have done much research on the CRRC [8-9] . The CRRC consists of a variable inlet guide vane (with 20 airfoils), the rotor-I (with 19 airfoils), the rotor-II (with 20 airfoils) and the outlet guide vane (with 32 airfoils). The design speed ratio of the CRRC was chosen to be 1 and the wheel speeds of the two counter-rotating rotors were 8000 and -8000 rpm respectively. The stage design total pressure ratio is 1.22 at a corrected mass flow rate of 6.4Kg/s. Both rotors configurations were modeled with the same tip clearance of 0.5mm. More details about the aerodynamic design and experimental measurement are given by Liu[10] and Chen[11].

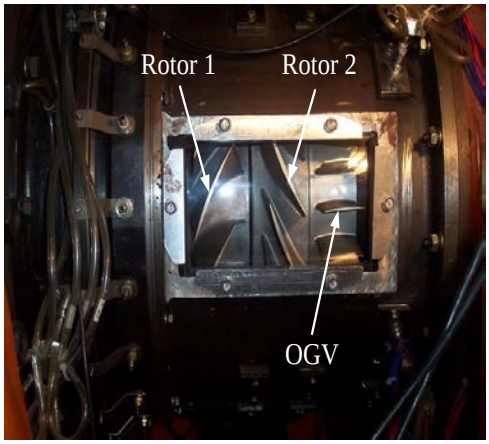

Fig. 1 View of the CAAC

V. DESCRIPTION OF THE NUMERICAL MODEL

The numerical simulation were undertaken with the commercial CFD code Fine™/Turbo of NUMECA, which has been extensively used for turbomachinery industry. Its continuous development over the years has extended its versatility to a number of aero-engines design applications.

The geometry of the CRRC has been partitioned using pre-processor Autogrid5. A structured O_4H mesh was generated for each blade passage, which is convenient for parallel computation. An O-grid is generated around the blade for a good control of the stretching in the direction normal to the wall. A butterfly grid topology and 33 grid points is applied in the tip clearance region of both rotors to model leakage effects accurately. The mesh is refined towards the solid boundaries to meet the requirements of the low-Reynolds turbulence model of $y+ < 5$. Since the NLH method works in the frequency domain, only one blade passage is needed. The number of grids in each of the rotor passages is listed in Table 1.

Past simulations of Vilmin [12] indicated that the number of grid points in the circumferential direction has to follow some strict guidelines. He suggested that there be at least 30 points in the circumferential direction for each harmonic. Furthermore, the number of grid points has to be weighted according to the number of blades on both sides of the rotor/rotor interface. Following his suggestions, the number of grid points in each of the blade passages is listed in Table 1. This grid density was deemed adequate for the purpose of this study.

Common grid has been subsequently used for the time-domain unsteady simulation to ensure consistency. While the original blade row number ratio is 20:19:20:32, for the time-domain unsteady simulation, it was necessary to change the blade row number ratio to 20:20:20:30. This simplification afforded a 1/1/1/2 model, which is a considerable reduction in computational resources. A modicum of scaling was used for rotor I and OGV to preserve the same solidities so that the blade loadings were approximately constant [13].

Prior to the NLH calculation, a single passage steady calculation with blade row interface mixing plane is carried out. For the steady flow, the governing equations are discretized in space using a cell-centered finite volume scheme together with the blend second-order and fourth-order artificial dissipation to damp numerical oscillations. Temporal integration of the governing equations is carried out using the explicit four-step Runge-Kutta scheme. The calculation is accelerated using local time-stepping and multi-grid techniques. The Reynolds stresses are closed by the S-A turbulence model because of its excellent stability.

At the inlet plane the measured total pressure and temperature quantities are imposed while the measured average static pressure was imposed at the exit plane. Non-slip and adiabatic conditions are adopted for all the solid walls. At blade row interface, unsteady disturbances for each blade row are obtained by a Fourier transform of pitchwise spatial nonuniformity of an adjacent blade row. The 1D non-reflecting boundary conditions are applied in order to prevent spurious reflections of outgoing waves back into the computational domain. The phase-shifted boundary conditions are used on the upper and lower periodical boundaries to solve the unsteady perturbation equations in a

single passage. It is essentially equivalent to the chorochronic conditions demonstrated by Gerolymos [14]. In the present simulation, the downstream running wake and upstream running potential wave is resolved by the first three harmonics.

The main drawback of the NLH method is that it requires much more memory compared to a typical time-domain unsteady simulation [12]. Considering this and in order to reduce computation time, we choose a cluster system to do the coarse-grained parallel simulation, which consists of 14 IBM BladeCenter HS21 nodes and runs in a Linux environment. Each node has 8GB memory size and 2-way 2 GHz Intel Xeon E5405 Quad core processors. Parallel Virtual Machine (PVM) and Open Message Passing Interface(OMPI) communication protocols are used for Interprocessor communication.

The time-domain unsteady method is based on the dual-time stepping approach of Jameson [19], where every instantaneous flow solution is considered as a "pseudo-steady" state problem. 40 physical time steps with 40 inner pseudo-time steps per Rotor 2 blade passing are used.

The entire operating range of the CRRC, from choke to near-stall conditions, is simulated with nine different mass flow rate values. Efficiency, mass flow, pressure ratio and residuals were monitored during the computations for assuring that the solution was converged. In terms of computational efficiency, the NLH method starting from a converged steady solution could be obtained in about 20-30 hours depending on the simulation point. This represents a big savings in computational time while the time-domain unsteady calculation needs about 20 hours for one period and at least 10 periods to obtain a periodic solution. Therefore, for this case, the NLH method is about one order magnitude faster than the direct time-domain method.

TABLE I NUMBER OF GRIDS FOR THE BLADE PASSAGE

	Pitchwise	Spanwise	Streamwise	Tip Grids
IGV	123	77	157	none
Rotor I	123	77	237	33
Rotor II	157	77	237	33
OGV	113	77	237	none

VI. COMPARISON WITH EXPERIMENTAL DATA

Figure 2 shows the experimentally measured performance maps along with the numerical results obtained using the present NLH method and time-average of unsteady simulation. The experimental values are area averaged quantities while the numerical simulations are mass averaged quantities. It can be seen that the total pressure ratio of both simulations is in good agreement with measured results, while isentropic efficiency is a little deviation from simulations. As analyzed by Chen, the measured efficiency have a measurement uncertainty which is dominated by temperature rise uncertainty [8]. It should be noted that the mass flow rate resulting from NLH simulation is larger than that from time-averaged unsteady simulation for the whole operating line. In design point the efficiency predicted by the NLH method is only 0.5% higher than that predicted by the time-averaged unsteady simulation. When the operating condition moves away from the design point, the discrepancy between them grows larger and is about 3% for the near stall condition. The discrepancy might stem from separated flow fields at near-stall condition, which exhibits strong nonlinear unsteady interactions and cannot be resolved with the NLH method with only three orders. As analyzed by He [16], conventional harmonic method using a pseudo-time-marching technique often exhibits solution divergence behavior for separated flow fields while it is often unavoidable for highly loaded design at near-stall conditions. In total, the satisfying results can be achieved with the NLH method in a fraction of time in contrast to a time-domain unsteady simulation although small discrepancies exist, also the NLH results are very accurately reproduced compared with the test data.

Figures 3 and 4 show profiles of the radial distribution of the mass-averaged absolute total pressure and isentropic efficiency at the exit plane of the CRRC for NLH method and unsteady simulation. The agreement between the two sets of results is also very good. Thus the NLH method provides a correct representation of the time-averaged flow field to the CRRC.

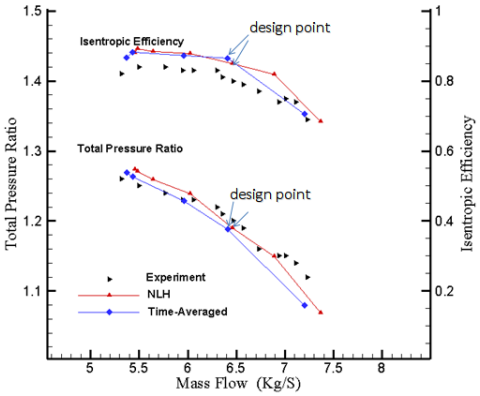

Fig.2 Comparison of experiment, NLH method and time-averaged unsteady characteristic

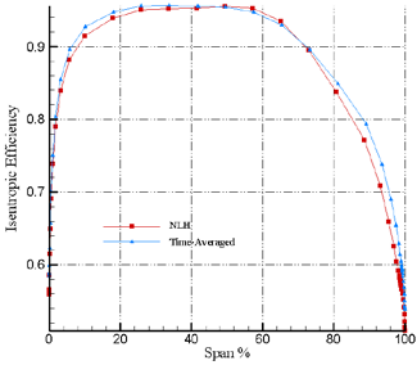

Fig.3 Spanwise distribution of isentropic efficiency

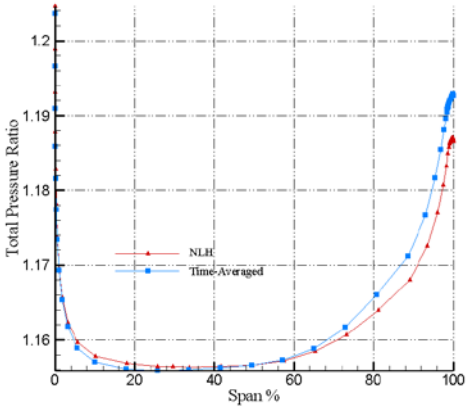

Fig. 4 Spanwise distribution of total pressure ratio

VII. INFLUENCE OF ROTOR-ROTOR INTERACTION

Comparisons of the NLH method and time-domain unsteady method of CRRC with steady simulation are carried out at the aero design point. Figure 5 shows the comparison of one-dimensional distributions of entropy along axial direction in the rotor I and rotor II passage respectively, which are area averaged for the whole S3 plane. The focus here is placed on the rotor/rotor interface. In steady simulation, only the averaged flux can be transferred through the interface, and the non-uniform flux is completely mixed out at the rotor I outlet boundary and subsequently transferred to the rotor II frame to provide uniform and steady inflow boundary conditions. Considerable loss is generated across the interface due to the mixing of wake blockage. The mixing loss at interface is removed by adding the deterministic stresses in the NLH method. It shows that there is little difference between the NLH and unsteady simulation in most of the axial positions. With three orders of perturbation, the NLH method can recover nearly 80% of the mixing loss. Continuity of the flow variables across the interface is exactly satisfied for an infinite number of time harmonics. Since the NLH method uses a limited number of harmonics, this continuity cannot be rigorously reproduced. But the observed continuity in the numerical results increases with a higher number of harmonics.

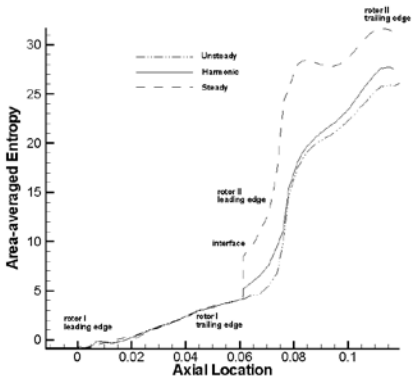

Fig. 5 Comparisons of 1-D entropy distribution along axial direction

Figure 6 with the inset shows the harmonic static pressure amplitude on rotor-II blade surface at 50% span of aero design point with first harmonic, second harmonic, and third harmonic. The first two orders of perturbations dominate the pressure amplitude, which is consistent with the previous analysis that the first three orders of unsteady perturbations can recover about 80% of the mixing loss.

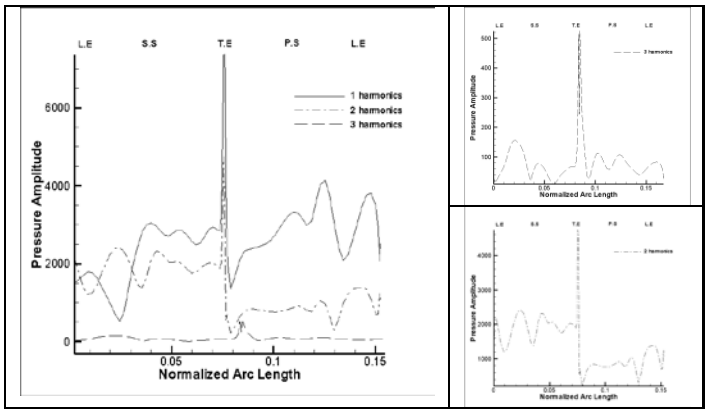

Fig. 6 Harmonic pressure amplitude on rotor-II blade surface at 50% span

Figure 7 shows the reconstructed instantaneous entropy contours at 50% span for rotor I, rotor II and OGV, as derived from the NLH method. The time increments are equally spaced over a cycle of the rotor-rotor period. The efforts in terms of mesh generation and the simulation configuration have allowed for a good resolution of the important flow phenomena. As can be seen in the figure, the flow field exhibits strong unsteady phenomena that are periodic in nature.

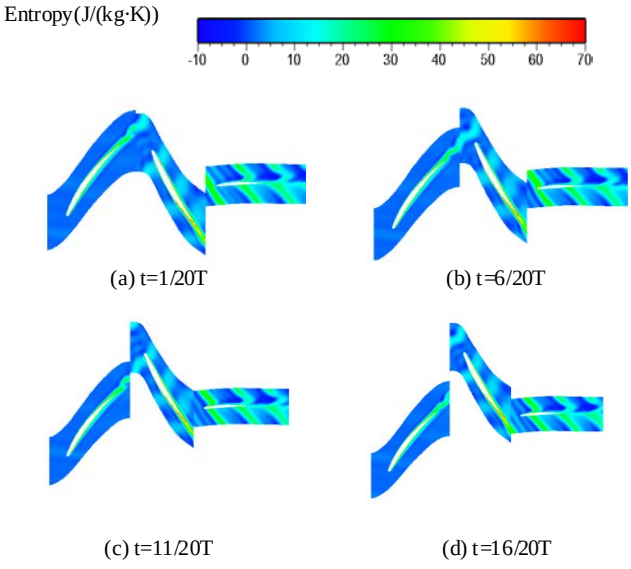

Fig. 7 Instantaneous entropy

The rotor I and rotor II wakes are clearly visible as regions of high entropy. At the given point of time, for example, t=1/20T, The wakes from rotor I are chopped at the rotor II blade leading edge and divided into two segments. The chopped wake segments propagate independently of each other within the adjacent rotor blade channels with the free stream velocity. Depending on the

solidity and speed ratio, several chopped rotor I wakes can be found within a single rotor II blade passage. For the rotor-rotor blade count and design wheel speeds of the CRRC, three to four rotor I wake segments appear within a single rotor II blade passage, depending on the point of time. The propagation velocity of the upstream wake segments is determined by the velocity distribution within the blade passages. For this reason, in the front part of the blades, the wake segments propagate faster near the suction surface than near the pressure surface. This is more evident in the OGV passages.

Once the rotor I wake are chopped by the rotor II and then propagate downstream inside, the low velocity inside the wake causes the low momentum wake to transport and collect near the pressure surface forming so called ‘‘negative jet’’ when the wake and entropy is transported downstream. This results in a local broadening of the wake segment near the pressure surface and a thinning near the suction surface. The characteristics of ‘‘negative jet’ is similar to a typical axial-flow compressor [21]. The magnitude of wake-induced unsteadiness depends on the spacing between the two rotors. With three orders of perturbation, the NLH method successfully captures the physical phenomenon of “wake stretching” inside the rotor II and OGV passage. It compares very well with the instantaneous entropy contours produced from the time-domain unsteady simulation (not shown).

Figures 8 and 9 show the rotor I and rotor II surface static pressure distributions at 50% span of aero design point. Time-averaged and reconstructed instantaneous values based on the phase-shifted periodicity are shown on the same plots. The time-averaged loading of rotor I is almost the same as the instantaneous loading except in the trailing edge. In design condition, the relative Mach number of the full span of the rotor II are subsonic, so there is no bow shock interaction with the upstream rotor wake, which means that pressure fluctuations on the rotor I are dominated by the rotor II potential fields as they propagate upstream the rotor I.

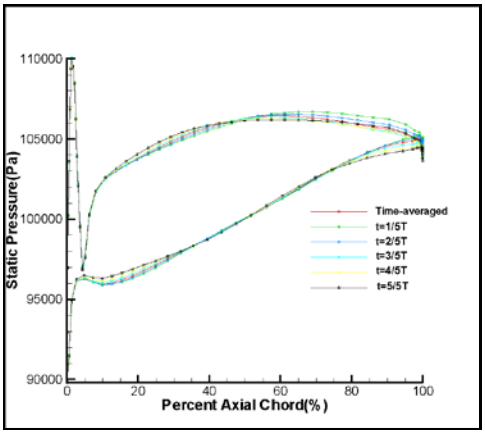

Fig. 8 Pressure fluctuations on rotor I surface

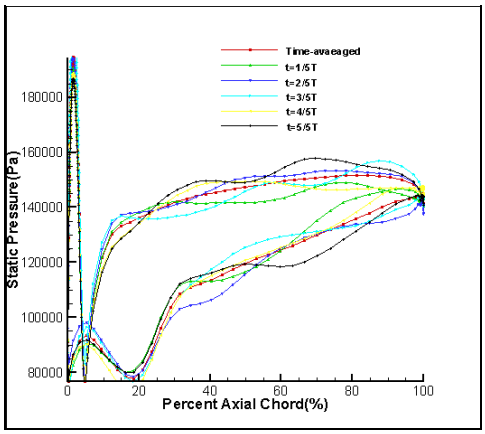

Fig. 9 Pressure fluctuations on rotor II surface

These fluctuations appear weak in comparison with the fluctuations of the loading on the rotor II. For the rotor II, larger fluctuations are observed, which is due to the impact of the wake of rotor I propagated downstream and the potential fields of OGV propagated downstream inside the rotor II passage. The wake-induced unsteadiness and circumferential variation of flow conditions in the rotor/rotor interface causes period fluctuations of inlet flow conditions for the rotor II. Overall, the rotor-rotor interaction can affect a range of 85% rotor I axial chord from trailing edge performance, while whole axial chord length on rotor II performance, which indicates that the interaction between rotor I and rotor II is significant.

VIII. DETERMINISTIC STRESSES STUDY

The deterministic stresses appear in the NLH method through time averaging of the periodic unsteadiness due to the unsteady interaction of the neighboring blades. The deterministic stress has been post-processed from NLH simulation and compared to the time-domain unsteady results. An averaging procedure based on the method of Hall [18] has been developed to determine the deterministic stresses from the time-averaged flow field of the unsteady simulation. A total of 40 snapshots in one blade passing period were processed. In these figures, only $\overline{(\rho v')v'}$ are presented due to the paper length limitation

Figure 10(a) shows the full deterministic stresses $\overline{(\rho v')v'}$ (the sum of three orders) for NLH method at 50% span for rotor I. It can be seen that at the inlet the deterministic stresses levels are very low, primarily because the axial spacing between IGV and rotor I is relatively large so the wake of IGV decay rapidly and totally mixed out at the interface. As the flow pass through the blade passage, higher levels begin to appear near the trailing edge, as a result of potential effects from the interaction with the downstream rotor. In circumferential direction, the deterministic stresses are not uniform and the gradients are large in some regions. This is contrast to the average passage equation proposed by Adamczyk [5] where the deterministic stresses are uniform across the circumferential direction because it is rather hard and time-consuming to take account for the circumferential distributions in the

blade passages. In Figure 10 (b) Fairly good agreement is obtained based on unsteady simulation compared to NLH method.

Figures 10(c) present the results for NLH method at 50% span for rotor II. It can be seen that the deterministic stresses in the rotor I and rotor II have the same magnitudes .The location of high concentrations of $\overline{(\rho v')v'}$ is observed on the rotor/rotor interface. The deterministic stresses reduce in strength as the flow moves downstream as the unsteadiness due to the Rotor I wake dissipates. As the flow passes through the blade passage, higher levels begin to appear in the rotor wake, presumably as a result of potential effects from the interaction with the downstream OGV. The unsteady simulation results present also high values upstream of the rotor II leading edge and the transport and development of the deterministic stress in the flow field, which shows a good match between the two methods. Also the comparisons have been achieved for all of the other deterministic stresses (not shown).

Figures 11 present the deterministic stresses for 99% span. The patterns of the predicted deterministic stresses near the tip regions were considerably different from the mid-span where the tip leakage vortex is instead the dominant source of unsteadiness, especially in rotor II. One of the striking features is that a significant source of high deterministic stresses begins roughly from the blade leading edge following the approximate trajectory of the tip clearance flow. The NLH method manages to reproduce the positions of the local extrema of the deterministic stresses in rotor I. However, in the leading edge of rotor II there is a noticeable difference in the quantitative results, partly because of the strong upstream wakes and rotor II tip clearance flow interaction, which has ever higher blade passing frequency and needs more orders of harmonics to simulate accurately.

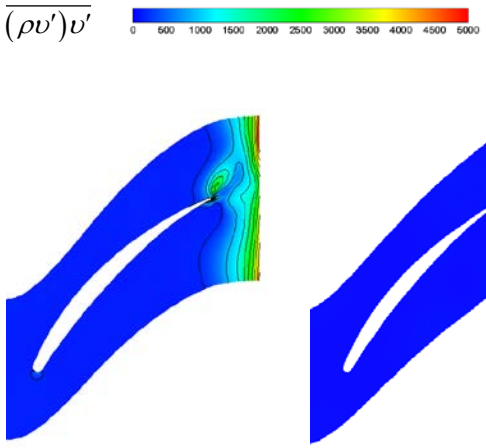

(a) r1 50%span (NLH method) (b) r1 50%span (Unsteady)

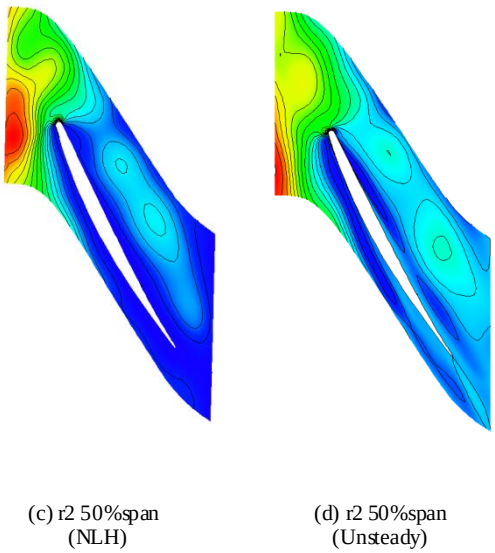

(c) r2 50%span (NLH) (d) r2 50%span (Unsteady)

Fig. 10 comparison of deterministic stress $\overline{(\rho v')v'}$ distribution at 50% span

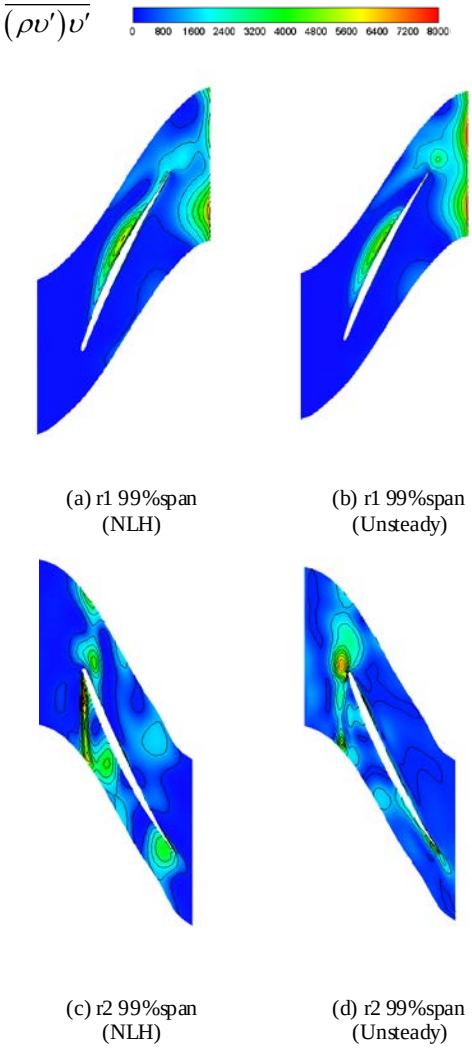

(a) r1 99%span (NLH) (b) r1 99%span (Unsteady)

(c) r2 99%span (NLH) (d) r2 99%span (Unsteady)

Fig. 11 comparison of deterministic stress $\overline{(\rho v')v'}$ distribution at 99% span

IX. CONCLUDING REMARKS

To investigate the capability of the NLH method on predicting unsteady flows induced by rotor-rotor interactions, the unsteady flows in a counter-rotating research compressor (CRRC) have been simulated. Starting from a steady solution, a converged solution with 3 harmonics could be obtained in about 20 hours on IBM BladeCenter HS21 using OMPI. The NLH method delivered accurate results at design points compared to time-domain unsteady results.

Analysis of the results provided some insight into the flow mechanism of rotor-rotor interaction, the following conclusions were drawn:

1. The NLH method takes at least one order of magnitude faster than typical time-domain unsteady simulations in terms of computational efficiency, which seems to be very promising for routine unsteady simulations in the design of modern multistage turbomachinery.

2. Comparative studies show that the present NLH method can capture the time-averaged results in good agreement with the time-domain unsteady method and experimental results, especially for the aero design point.

3. With the three orders of wake and potential perturbations included, 90% mixing loss could be recovered at the rotor/rotor interface.

4. The NLH method has proven to resolve and sustain rotor-rotor interaction phenomena quite well. In the present test case, the primary contributor to the deterministic stresses at mid-span is the interaction of a blade with the upstream rotor wakes while the tip leakage flow is the dominant source of unsteadiness and deterministic stresses in the tip region.

The achieved results are a valuable enlargement of a data base in order to design counter rotating compressor with higher performance.

REFERENCES

[1] S. M. Metev and V. P. Veiko, *Laser Assisted Microtechnology*, 2nd ed., R. M. Osgood, Jr., Ed. Berlin, Germany: Springer-Verlag, 2005.

[2] S. Zhang, C. Zhu, J. K. O. Sin, and P. K. T. Mok, "A novel ultrathin elevated channel low-temperature poly-Si TFT," *IEEE Electron Device Lett.*, vol. 20, pp. 569–571, Nov. 2007.

[3] M. Wegmuller, J. P. von der Weid, P. Oberson, and N. Gisin, "High resolution fiber distributed measurements with coherent OFDR," in *Proc. ECOC'00*, 2000, paper 11.3.4, p. 109.

[4] R. E. Sorace, V. S. Reinhardt, and S. A. Vaughn, "High-speed digital-to-RF converter," U.S. Patent 5 668 842, Sept. 16, 2007.

[5] (2002) The IEEE website. [Online]. Available: http://www.ieee.org/.

[6] M. Shell. (2002) IEEEtran. homepage on CTAN.

[7] http://archive/macros/latex/contrib/supported/IEEEtran/.

[8] *FLEXChip Signal Processor (MC68175/D)*, Motorola, 2010.

[9] "PDCA12-70 data sheet," Opto Speed SA, Mezzovico, Switzerland.

[10] A. Karnik, "Performance of TCP congestion control with rate feedback: TCP/ABR and rate adaptive TCP/IP," M. Eng. thesis, Indian Institute of Science, Bangalore, India, Jan. 2009.

[11] J. Padhye, V. Firoiu, and D. Towsley, "A stochastic model of TCP Reno congestion avoidance and control," Univ. of Massachusetts, Amherst, MA, CMPSCI Tech. Rep. 99-02, 2008.

[12] J. Breckling, Ed., The Analysis of Directional Time Series: Applications to Wind Speed and Direction, ser. Lecture Notes in Statistics. Berlin, Germany: Springer, 2008, vol. 61.